17th International Conference on the Application of Computer
Science and Mathematics in Architecture and Civil Engineering
K. Gürlebeck and C. Könke (eds.)
Weimar, Germany, 12–14 July 2006

ADAPTIVE SIMULATION OF THE DAMAGE BEHAVIOR OF CONCRETE USING HETEROGENEOUS MULTISCALE MODELS

S. Eckardt[*], **C. Könke**

[*]*Institute of Structural Mechanics, Bauhaus-University Weimar*
Marienstrasse 15, Weimar, Germany
E-mail: stefan.eckardt@bauing.uni-weimar.de

Keywords: concrete, multiscale, damage mechanics, adaptivity.

Abstract. *In this paper an adaptive heterogeneous multiscale model, which couples two substructures with different length scales into one numerical model is introduced for the simulation of damage in concrete. In the presented approach the initiation, propagation and coalescence of microcracks is simulated using a mesoscale model, which explicitly represents the heterogeneous material structure of concrete. The mesoscale model is restricted to the damaged parts of the structure, whereas the undamaged regions are simulated on the macroscale. As a result an adaptive enlargement of the mesoscale model during the simulation is necessary.*

In the first part of the paper the generation of the heterogeneous mesoscopic structure of concrete, the finite element discretization of the mesoscale model, the applied isotropic damage model and the cohesive zone model are briefly introduced. Furthermore the mesoscale simulation of a uniaxial tension test of a concrete prism is presented and own obtained numerical results are compared to experimental results. The second part is focused on the adaptive heterogeneous multiscale approach. Indicators for the model adaptation and for the coupling between the different numerical models will be introduced. The transfer from the macroscale to the mesoscale and the adaptive enlargement of the mesoscale substructure will be presented in detail. A nonlinear simulation of a realistic structure using an adaptive heterogeneous multiscale model is presented at the end of the paper to show the applicability of the proposed approach to large-scale structures.

1 INTRODUCTION

Concrete is showing a macroscopic damage behavior, which is the result of the initiation, propagation and coalescence of microcracks within the heterogeneous structure of the material on the mesoscale. The influence of the material heterogeneity is often neglected during the nonlinear analysis of concrete structures and a homogeneous isotropic or anisotropic material behavior is assumed. Complex constitutive models as for example shown in Jirásek and Bažant [1], Bažant and Planas [2] or Hofstetter and Mang [3] can be used to simulate the deterioration behavior of concrete under tension and compression. Because most of the internal material parameters can not be measured directly in physical experiments, the identification of the material parameters is generally difficult.

In a new approach it is proposed to use mesoscale models for the nonlinear analysis of concrete [4, 5]. On the mesoscale the numerical model explicitly represents the components of the heterogeneous structure of the composite material. Three main components: coarse aggregates with diameters greater than 2 mm, mortar matrix (cement paste, voids and aggregates with diameters smaller than 2 mm) and the interfacial transition zone (ITZ) between them are generally considered on the mesoscale. A homogenization is only required for each component with less heterogeneity compared to the macroscopic composite. As a result rather simple material models can be used for each constituent of the mesoscale model, to describe the complex macroscopic material behavior [6]. Furthermore effects such as the evolution of microcracks or the debonding of the ITZ are explicitly represented by mesoscale models. A localization of damage, that is typical for concrete structures, automatically occurs due to the heterogeneity of the material.

In the presented approach the nonlinear material behavior of concrete is restricted to tensile failure within the mortar matrix and debonding effects within the ITZ. It is assumed, that compressive failure on the macroscale can be reduced to tensile failure perpendicular to the direction of the principal compressive stress on the mesoscale. Furthermore the nonlinear material behavior of the aggregates is neglected and a linear elastic material model is associated to them.

Simulations with mesoscale models require fine resolutions of the discretized model, leading to models with a large number of degrees of freedom. Therewith the analysis of realistic structures only with mesoscale models is not feasible with today's computational power. Knowing that damage in concrete normally localizes in small regions compared to the geometrical dimensions of the macroscopic structure a heterogeneous multiscale model can be used to reduce the numerical effort. In these models only regions with localized large damage zones are simulated on the mesoscale, whereas macroscale models are used for the undamaged or sparsely damaged regions. In realistic large-scale structures the damage distribution is generally not known in advance and an adaptation of the multiscale model during the simulation is required. In this paper the model adaptation is restricted to a conversion from the macro- to the mesoscale.

2 MESOSCALE MODEL

2.1 Geometrical representation

One requirement for mesoscale simulations is an appropriate representation of the mesoscopic geometry, e.g. the particle arrangement, of the composite material. In the presented paper the heterogeneous meso-scale geometry of concrete is generated using numerical simula-

tions. The generation algorithm will be briefly introduced in the following paragraphs. A more detailed description can be found in [6] and [7].

The simulation starts with the generation of the aggregates, which are represented by ellipsoids. Equation 1 describes the surface of an ellipsoid as a function of the three diameters $d_1,\ d_2$ and d_3, whereby $d_1 \geq d_2 \geq d_3$.

$$\left[\frac{2 \cdot x}{d_1}\right]^2 + \left[\frac{2 \cdot y}{d_2}\right]^2 + \left[\frac{2 \cdot z}{d_3}\right]^2 = 1 \tag{1}$$

The simulated aggregates should statistically match a given mass fraction and size distribution. For concrete the aggregate size distribution is characterized by grading curves, which are obtained by a sieve analysis. As a result the aggregates are divided into several mineral-size-classes, which are bounded by a lower diameter d_{min} and an upper diameter d_{max}. In the presented approach the sieve passing of an aggregate is only defined by the second largest diameter d_2. Assuming a linear function within one mineral-size-class in the semi-logarithmic diagram of a grading curve, as shown in Figure 1, d_2 is calculated using equation:

$$d_2 = \frac{d_{min} \cdot d_{max}}{\sqrt[3]{X_1 \cdot d_{min}^3 + (1 - X_1) \cdot d_{max}^3}} \tag{2}$$

where X_1 denotes a uniformly distributed random number between 0 and 1. The diameters d_1 and d_3 are than calculated as a function of d_2:

$$d_1 = \left[1 + X_2 \cdot \frac{r_{13} - 1}{r_{13} + 1}\right] \cdot d_2 \tag{3}$$

$$d_3 = \left[1 - X_3 \cdot \frac{r_{13} - 1}{r_{13} + 1}\right] \cdot d_2 \tag{4}$$

where X_2 and X_3 are uniformly distributed random numbers between 0 and 1 and the parameter r_{13} defines the maximum ratio between the diameters d_1 and d_3.

After the desired mass fraction is reached, all aggregates are sorted by their volume. Then they are randomly placed within the specimen geometry one by one starting with the aggregate with the largest volume. Uniformly distributed random numbers are used for the calculation of the position (center point coordinates) and the orientation (Eulerian angles) of the ellipsoid. Separation checks are performed to prevent overlapping of the aggregates. In a first step the bounding boxes of the ellipsoids are tested. If this test fails, an exact separation check, which is based on a very efficient algorithm introduced by [8], is performed. If the exact test also fails, a new position and orientation for the ellipsoid is chosen and the separation checks are repeated, until both tests are passed.

The result of the presented algorithm is one sample of a three-dimensional aggregate distribution. Intersections between the specimen and a plane are used for two-dimensional simulations of the material response, leading to aggregates, which are then represented by ellipses.

A small example of a concrete cube with edge length of 100 mm is presented in the next paragraph to show the performance of the algorithm. The prescribed grading curve is given in Figure 1 and the following parameters are assumed: mass density of aggregates: $\varrho_a = 2.67\mathrm{t/m^3}$, mass density of macroscopic concrete: $\varrho_c = 2.30\mathrm{t/m^3}$, mass fraction of aggregates: $\varphi_a = 80\,\%$, maximum ratio between the ellipsoidal diameters d_1 and d_3: $r_{13} = 3$.

Altogether approximately $320,000$ aggregates with diameters between 0.5 mm and 32.0 mm are generated within the cube. The volume fraction of all simulated aggregates is $62\,\%$, which

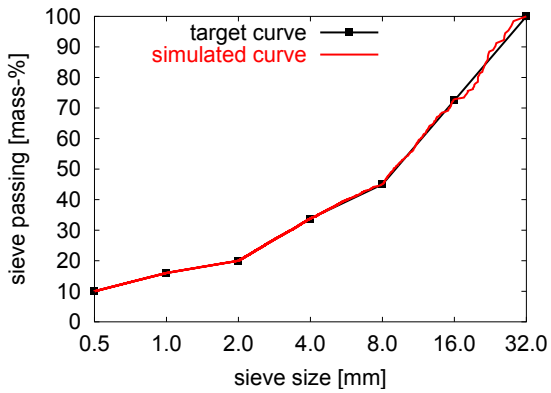

Figure 1: Prescribed and generated grading-curve.

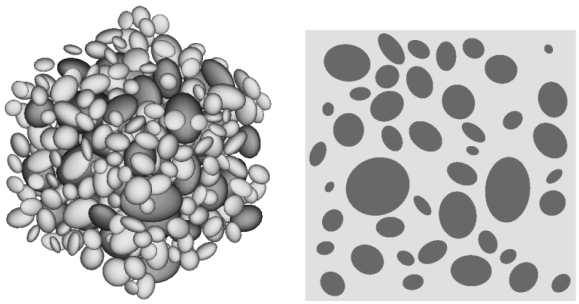

(a) 3D (b) 2D

Figure 2: Simulated aggregate distribution.

is equivalent to the prescribed mass fraction. This process takes approximately 90 seconds on a standard PC. The diagram (Fig. 1) illustrates, that the generated aggregates statistically fits the given size distribution for a sufficiently large number of ellipsoids. Figure 2(a) shows the three-dimensional aggregate arrangement of the mineral-size-classes 8/16 (321 ellipsoids, light-gray) and 16/32 (40 ellipsoids, dark-gray). The result of an intersection between the cube and a plane parallel to the base of the cube is plotted in Figure 2(b). Only aggregates with diameters greater than 8 mm are shown in the plot. The area fraction of the aggregates in this cross-section is $35\ \%$.

2.2 Numerical model

For numerical simulations the components of the mesoscale geometry are discretized using solid finite elements. The finite element mesh explicitly represents the boundaries between aggregates and matrix. As a result zero-thickness interface elements can be applied between them to model the interfacial transition zone. In the presented paper the numerical simulations are restricted to two-dimensional plane stress models using triangular finite elements, with linear or quadratic interpolation functions.

Due to the complexity of the mesoscale geometry the numerical effort for mesh generation is very high and it increases with the numbers of aggregates embedded in the mortar matrix. A minimum distance between two aggregates and between an aggregate and the specimens boundary surface is introduced to reduce the numerical effort for mesh generation and to prevent very small or highly distorted finite elements. As a result the numerical effort for the generation of the mesoscale geometry increases. Furthermore the volume fraction of the aggregates has to be reduced to guarantee that all ellipsoids can be placed within the specimen without using a compaction algorithm.

In the presented approach the nonlinear material behavior of concrete is restricted to debonding of the ITZ and tensile failure within the mortar matrix, which means the initiation, propagation and coalescence of microcracks. It is assumed, that compressive failure on the macroscale can be reduced to tensile failure perpendicular to the direction of the compressive stress on the mesoscale. Furthermore the nonlinear material behavior of the aggregates is neglected and a linear elastic material model is associated to them.

2.2.1 Isotropic damage model

In this paper the nonlocal formulation of the isotropic continuum damage model, described by [9] is used, to simulate the evolution of microcracks within the mortar matrix. The material model is fully characterized by five material parameters: the Young's modulus E, the Poisson's ratio ν, the tensile strength f_t, the fracture energy G_f and the nonlocal interaction radius R. In this model the damage state of the material is expressed by a scalar parameter ω ranging from 0 to 1, whereby $\omega = 0$ indicates the undamaged state and $\omega = 1$ represents a fully damaged material. The constitutive equation is given by:

$$\boldsymbol{\sigma} = (1 - \omega)\boldsymbol{C}_{el} : \boldsymbol{\varepsilon} \tag{5}$$

where $\boldsymbol{\sigma}$ is the stress tensor, $\boldsymbol{\varepsilon}$ the strain tensor and $\boldsymbol{C}_{el}$ the linear elastic material tensor. The evolution of the damage parameter ω is given by the following exponential damage law:

$$\omega(\kappa) = \begin{cases} 0.0 & \kappa < \varepsilon_0 \\ 1.0 - \dfrac{\varepsilon_0}{\kappa} \exp\left(-\dfrac{\kappa - \varepsilon_0}{\varepsilon_f - \varepsilon_0}\right) & \kappa \geq \varepsilon_0 \end{cases} \tag{6}$$

whereby $\varepsilon_0 = f_t/E$ is the elastic limit, $\varepsilon_f = 2G_f/f_t$ is a parameter which controls the ductility of the material and κ is a history variable that is related to the maximum equivalent strain ε_{eq} ever reached in the material history. In the presented version of the isotropic damage model the Rankine criterion is used for damage initiation. As a result the equivalent strain has to be calculated using the following equation:

$$\varepsilon_{eq} = \frac{1}{E} \max_{i=1,2,3} \sigma_{el,i} \tag{7}$$

where $\sigma_{el,i}$ is the i-th eigenvalue of the elastic stress tensor which is defined as a function of the nonlocal strain $\boldsymbol{\varepsilon}_{nl}$:

$$\boldsymbol{\sigma}_{el} = \boldsymbol{C}_{el} : \boldsymbol{\varepsilon}_{nl} \tag{8}$$

The nonlocal strain $\boldsymbol{\varepsilon}_{nl}$ is calculated as the weighted average of the local strain field $\boldsymbol{\varepsilon}$ using the following equations:

$$\alpha_0(r) = \begin{cases} 0.0 & r > R \\ \left[1 - \dfrac{r^2}{R^2}\right]^2 & r \leq R \end{cases} \tag{9}$$

$$\alpha(r) = \frac{\alpha_0(r)}{\displaystyle\int_V \alpha_0(r)\,\mathrm{d}V} \tag{10}$$

$$\boldsymbol{\varepsilon}_{nl}(\boldsymbol{x}) = \int_V \alpha(\|\boldsymbol{x} - \boldsymbol{\xi}\|)\ \boldsymbol{\varepsilon}(\boldsymbol{\xi})\,\mathrm{d}V \tag{11}$$

where r is the distance between the point with coordinates $\boldsymbol{\xi}$, and the integration point, with coordinates $\boldsymbol{x}$. The weight function, given in Equation 9 is a truncated polynomial bell-shaped function. As a result the nonlocal average is restricted to the vicinity of the integration point. The integrals given in Equations 10 and 11 are numerically solved using the integration points of the finite elements.

A consistent tangential stiffness matrix is calculated for the presented nonlocal isotropic damage model. The matrix is generally unsymmetric and the bandwidth of the matrix is growing during simulation depending on the damage distribution within the numerical model [10]. As a result the numerical effort for the calculation of the stiffness matrix and the memory demand for storing the matrix is increasing during the simulation. Using the consistent tangential stiffness matrix within the global Newton-Raphson iteration procedure a quadratic rate of convergence can be observed. Compared to a local formulation of the isotropic damage model the nonlocal formulation shows a considerably better convergence behavior, assuming that a sufficiently large number of integration points are used for the nonlocal averaging of the strains [9]. The very efficient sparse direct solver MUMPS [11] is used in our finite element system SLang to solve the global system of equations.

2.2.2 Interface damage model

A cohesive zone model, based on Tvergaard [12] is used to describe the nonlinear material behavior within the interfacial transition zone between aggregates and matrix. In these kind of models the constitutive relations between the normal and tangential tractions T_n and T_t and the coressponding displacement differences across the interface Δu_n and Δu_t are expressed by a nonlinear traction-separation law. The used interface model is briefly introduced in the following paragraphs. A more detailed description can be found in [13].

An equivalent interface opening λ is defined as:

$$\lambda = \sqrt{\Delta u_n^2 + (\alpha \cdot \Delta u_t)^2} \tag{12}$$

where α is a material parameter, that controls the weighting between the normal and tangential opening of the interface. The nonlinear traction-separation law, describing the relationship between the equivalent interface opening and the equivalent traction σ, is chosen as:

$$\sigma(\lambda) = \begin{cases} K_p \cdot \lambda & \lambda < \lambda_0 \\ f_{ct} \cdot \exp \dfrac{-f_{ct} \cdot (\lambda - \lambda_0)}{G_f} & \text{otherwise} \end{cases} \tag{13}$$

whereby $\lambda_0 = f_{ct}/K_p$ defines the elastic limit, K_p is the penalty stiffness, f_{ct} the tensile strength of the interface and G_f its fracture energy.

Assuming, that the constitutive relations of the interface are derived from a potential Φ specified by:

$$\Phi = \int_0^{\lambda} \sigma(\lambda') \mathrm{d}\lambda' \tag{14}$$

the normal and tangential tractions are given by:

$$T_n = \frac{\partial \Phi}{\partial \Delta u_n} = \sigma(\lambda) \cdot \frac{\Delta u_n}{\lambda} \tag{15}$$

$$T_t = \frac{\partial \Phi}{\partial \Delta u_t} = \sigma(\lambda) \cdot \frac{\alpha^2 \cdot \Delta u_t}{\lambda} \tag{16}$$

Equation (13) applies for an increasing λ, ($\dot{\lambda} > 0$), and $\lambda = \lambda_{max}$, whereby λ_{max} is a history variable describing the maximum equivalent interface opening reached during the loading

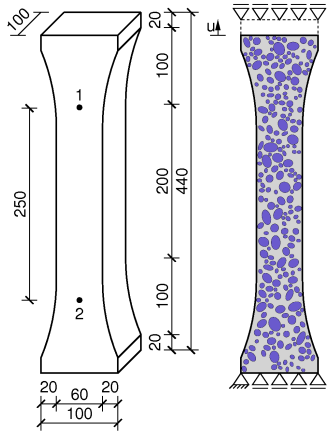

Figure 3: concrete prism: specimen dimensions, monitoring points, mesoscale geometry and boundary conditions.

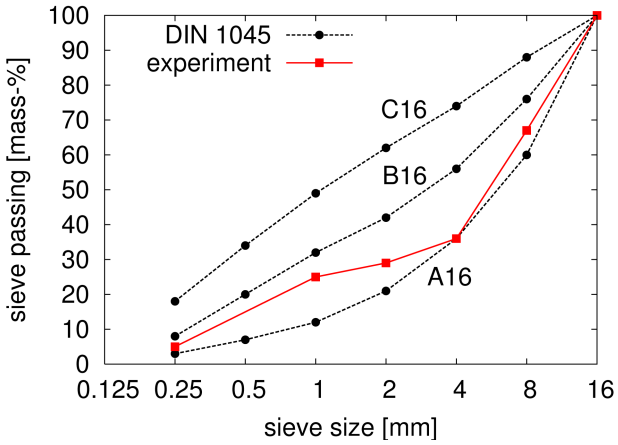

Figure 4: concrete prism: grading curve used in the experiments and grading curves defined by the German standard DIN 1045.

process. For decreasing λ an elastic unloading to the origin is assumed:

$$T_n = \sigma(\lambda_{max}) \cdot \frac{\Delta u_n}{\lambda_{max}} \tag{17}$$

$$T_t = \sigma(\lambda_{max}) \cdot \frac{\alpha^2 \cdot \Delta u_t}{\lambda_{max}} \tag{18}$$

In compression equation (12) reduces to:

$$\lambda = |\alpha \cdot \Delta u_t| \tag{19}$$

and the contact condition is approximated by the penalty stiffness:

$$T_n = K_p \cdot \Delta u_n \tag{20}$$

The value of the penalty stiffness, which controls the penetration of the two interface sides under compression, has to be chosen carefully, since a too large value results in an ill-conditioned stiffness matrix.

2.3 Example

The first example presented in this paper illustrates the numerical simulation of a concrete prism under uniaxial tensile loading using a mesoscale model. This specimen was experimentally tested by [14] at the University of Karlsruhe. Figure 3 shows the specimen dimensions, the position of the two monitoring points and the boundary conditions. The load was applied under displacement control at the top of the specimen. In the diagram shown in Figure 4 the grading curve which was used for the preparation of the specimens is plotted. For comparison the standard grading curves, defined by the german standard DIN 1045, are also plotted in this diagram. The mass of the aggregates is $1850\ kg$ (split into the mineral-size classes: 0/2 - $555\ kg$, 2/8 - $703\ kg$ and 8/16 - $592\ kg$) and a final concrete mass of $2300\ kg$ is assumed for $1\ m^3$ concrete.

One realization of a numerically generated mesoscale geometry, based on this mixture properties (grading-curve, mass of aggregates and mass of concrete) is shown in Figure 3. In this model only aggregates with diameters larger than $4\,mm$ are considered. The mesoscale geometry is discretized with 6-node triangular finite elements (assuming plane stress), with an average

Table 1: concrete prism: material parameters

			aggregates	mortar matrix		ITZ
			simulation 1+2	simulation 1	simulation 2	simulation 2
Young's modulus	E	$[N/mm^2]$	63,818	31,909	31,909	500,000
Poisson's ratio	ν	[–]	0.18	0.18	0.18	–
Tensile strength	f_{ct}	$[N/mm]$	–	4.00	4.47	3.40
Fracture energy	G_f	$[Nmm/mm^2]$	–	0.09	0.25	0.10
Nonlocal radius	R	$[mm]$	–	1.0	1.0	–

element size of $0.5\ mm$. This results in a finite element mesh consisting of 263,396 elements, 528,965 nodes and 1,057,131 active degrees of freedom. Two simulations are performed to investigate the influence of the ITZ. In simulation 1 rigid bond between aggregates and matrix is assumed. The nonlinear behavior of the ITZ is taken into account in simulation 2. In both simulations a linear elastic material behavior of the aggregates is assumed and the isotropic damage model is used for the mortar matrix. The material parameters, summarized in Table 1, are fitted to the experimental results, such that the peak load and the initial stiffness of the experimental curve is obtained.

The diagram in Figure 5 shows the stress-strain relationship for one experiment and for both simulations. The strain is calculated from the vertical displacements u_v measured at the monitoring points:

$$\varepsilon = \frac{u_{v,2} - u_{v,1}}{250\ mm} \tag{21}$$

For this uniaxial tensile test the stress is computed from the vertical reaction force R_v measured at the top of the specimen:

$$\sigma = \frac{R_v}{100\ mm \cdot 60\ mm} \tag{22}$$

Due to the parameter fitting of the material parameters, both simulations can represent the peak load. But simulation 2 shows a better approximation of the entire experimentally investigated curve. Assuming rigid bond, the pre-peak behavior of the material is overestimated and the calculated strain at the peak-point is too small. A comparison of the simulated post-peak behavior

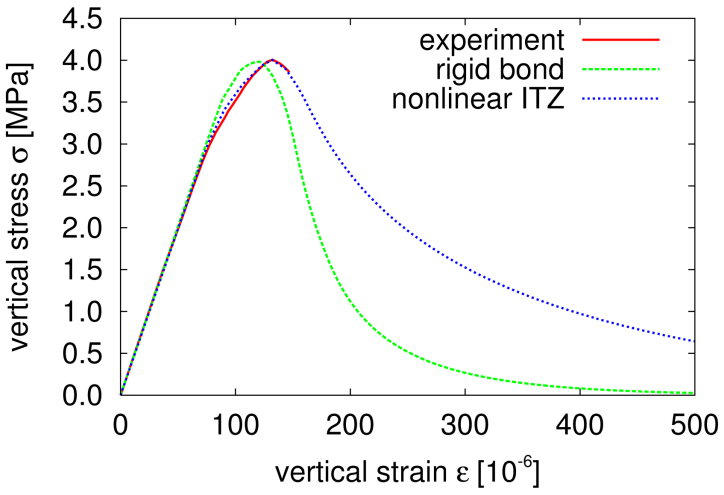

Figure 5: stress strain relationship.

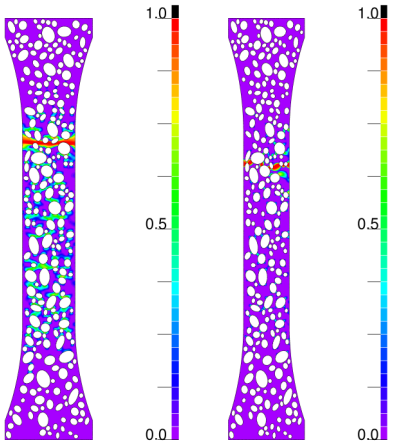

(a) sim. 1 (b) sim. 2

Figure 6: damage distribution.

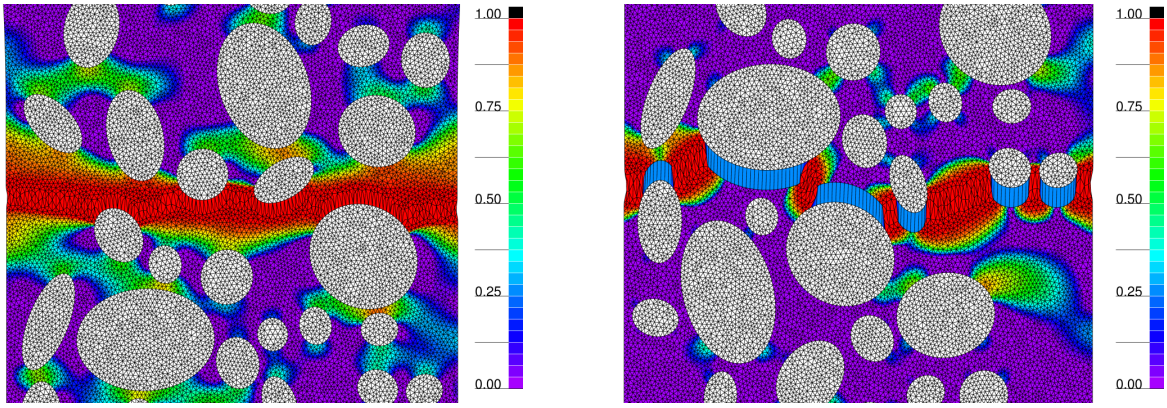

(a) simulation 1 (b) simulation 2

Figure 7: damage distribution within the localized region (displacements 10-times magnified).

with the physical experimental results is not possible, since the experiments became unstable after reaching the peak load [14].

Figure 6 shows the damage distribution for the entire mesoscale model. In these plots the localization of damage within a small region compared to the macroscopic dimension of the specimen is clearly visible. The position of the localization zone depends highly on the distribution of the aggregates, but is also influenced by the material behavior, assumed for the ITZ. A detailed plot of the damage distribution within this localized zones is shown in Figure 7. Both models can represent the initiation, propagation and coalescence of microcracks. Assuming rigid bond, Figure 7(a), interface cracks between aggregates and matrix have to be simulated as damage zones within the mortar matrix. This results in an enlargement of the damage zones around the aggregates. Using interface elements between aggregates and matrix, Figure 7(b), and assuming that the ITZ is the weak link within the material structure, the debonding effects within the ITZ are represented by the interface damage model. Only cracks bridging from aggregate to aggregate are simulated with the isotropic damage model, associated to the mortar matrix. Due to the predefined crack paths around the aggregates, simulation 2 shows a significantly better convergence behavior during the simulation compared with simulation 1.

3 MULTISCALE MODEL

3.1 Heterogeneous multiscale approach

As shown in the last preceding section, numerical simulations using mesoscale models require a very fine resolution of the structure. This results in large numbers of finite elements, nodes and degrees of freedom respectively. The numerical effort and the memory demand for the simulation of full large-scale engineering structures on the mesoscale cannot be handled with today's computational power.

Knowing that damage in concrete normally localizes in small regions compared to the geometrical dimensions of the macroscopic structure a heterogeneous multiscale model can be used to reduce the numerical effort. In these models only the damaged regions are simulated on the mesoscale, whereas macroscale models are used for the undamaged or sparsely damaged regions. As exemplary shown in Figure 8 there are several submodells with different scales of

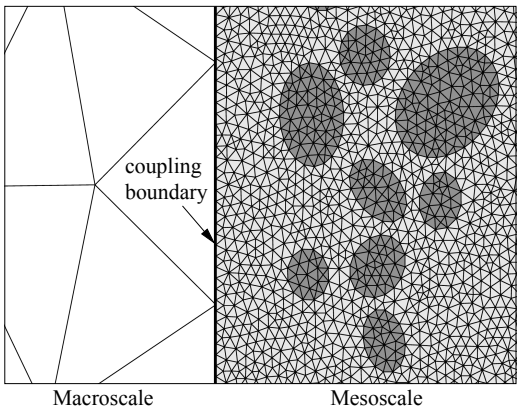

Figure 8: Heterogeneous multiscale approach.

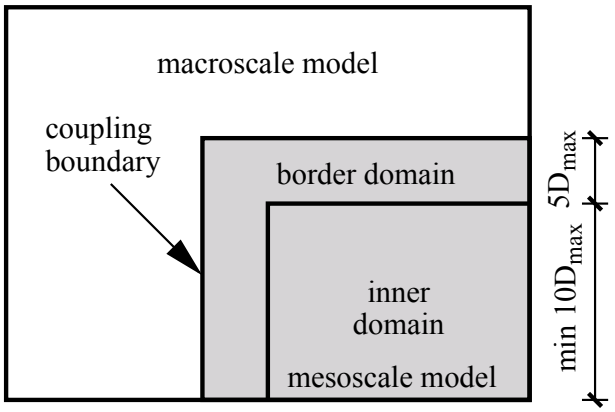

Figure 9: Heterogeneous multiscale model: mesoscale domains.

resolution within one numerical model, the so-called heterogeneous multiscale model.

In the presented approach the different submodels are coupled by constraint equations along the common domain boundaries enforcing displacement compatibility. On the common edge the mesoscale nodal degrees of freedom are expressed by macroscale nodal degrees of freedom. This kind of coupling overestimates the stiffness of the system and results in a spurious initiation of damage in regions where aggregates are close to the mesoscale boundary. A small zone of mortar matrix elements is introduced within the mesoscale models between the coupling boundary and the first aggregate elements to prevent spurious damage initiation. The width of the zone depends on the finite element discretization of the mortar matrix. This zone has to be large enough to uniformly distribute the constraint forces from the coupling into the mesoscale model. First simulations have shown that for triangular elements with quadratic interpolation functions a transfer zone of two matrix elements is large enough to prevent spurious damage initiation effects.

3.2 Model adaptation

In the presented heterogeneous multiscale model the nonlinear material behavior of concrete is only simulated within the mesoscale part of the model. In realistic large-scale structures the damage distribution is generally not known in advance and an adaptation of the multiscale model during the simulation becomes necessary.

In this paper the model adaptation is restricted to a conversion from the macroscale to the mesoscale. The macroscopic stress distribution and the mesoscopic damage evolution are used as indicators for a model adaptation. As a result stress concentrations on the macroscale and a localization of damage on the mesoscale is required. In the case of a homogeneous macroscopic stress field the adaptation process would result in a mesoscale model of the entire structure and a model adaptation from meso- to macroscale has to be performed. Furthermore the presented multiscale model is restricted to one mesoscale domain, which means that the initial mesoscale domain is enlarged during the simulation.

As a first step the mesoscale geometry, i.e. the aggregate distribution, is generated within the macroscopic structure. The simulation starts with a linear elastic analysis of the complete structure on the macroscale. Then the element with the largest principal stress value is chosen. All elements within a square, edge length $15\ D_{max}$, where D_{max} is the diameter of the largest aggregate, in the vicinity of the selected element are transferred to the mesoscale. The

outer boundary of this element patch is calculated and all aggregates within the boundary are selected. Then the finite element mesh of the new mesoscale substructure is generated using the program Gmsh [15]. The new mesoscale model replaces the indicated macroscale element patch and constraint equations are applied on the common boundary between the substructures. The nonlinear analysis of the structure starts with this initial multiscale model.

The evolution of the damage parameter ω is chosen as an indicator for the enlargement of the mesoscale substructure. As shown in Figure 9 the mesoscale model is divided into the border domain, containing all elements with a maximum distance of $5\,D_{max}$ from a coupling boundary, and an inner domain, which is built by all elements which are not in the border domain. The initiation and evolution of damage is limited to the elements within the inner domain. If damage initiates in an element within the border domain this element is selected, the simulation is stopped and an enlargement of the mesoscale model is performed. If damage initiates in more than one element within the border domain, the element with the largest damage value is chosen.

In a first step of the enlargement process all macroscale elements within a square, edge length $15\ D_{max}$, around the selected mesoscale element are chosen and the outer boundary of the macroscale element patch is calculated. Then the common boundary segments between the indicated macroscale element patch and the existing mesoscale model are determined. In a second step all mesoscale elements with a maximum distance of $2\ D_{max}$ from the previously determined common boundary segments are selected and a mesoscale element patch is built. A second condition for the selection of the mesoscale elements is, that an aggregate is either completely within or completely outside the selected mesoscale element patch. The combination of both element patches, macroscale elements and mesoscale elements, builds the new mesoscale domain which is later added to the existing domain.

Now the outer boundary of the selected elements is calculated and all aggregates within the boundary are determined. After that the finite element mesh of the new mesoscale domain is generated. A linear elastic analysis of this submodel is performed to obtain a displacement solution, which can be used as first prediction for the following iterative solution. Therefore the displacements from the last converged iteration step are applied to the boundary of the submodel. In the presented approach no further history variables have to be transferred between the old macroscale region and the new mesoscale submodel because linear elastic material behavior is assumed for the macroscale region, which therefore shows no damage before it is transferred to the mesoscale.

As a last step of the enlargement the selected old elements are deleted, the new submodel is added to the existing mesoscale model, the border and the inner domain is updated and constraint equations are applied between the substructures. A Newton Raphson iteration is performed to bring the entire multiscale model into global equilibrium for the current load level. The enlargement of the mesoscale substructure is repeated until no damage initiates in the border region. After the adaptation process is finished the nonlinear simulation is continued with the next load increment.

3.3 Example

The example shows the nonlinear analysis of a L-shaped panel that was experimentally tested by Winkler [16] at the University of Innsbruck. In Figure 10 the specimen geometry and the test setup is reproduced.

A nonlinear analysis of the specimen under a displacement controlled loading is performed in a first simulation for a pure macroscale model and in a second simulation for an adaptive heterogeneous multiscale model. The nonlocal isotropic damage model is applied to all elements

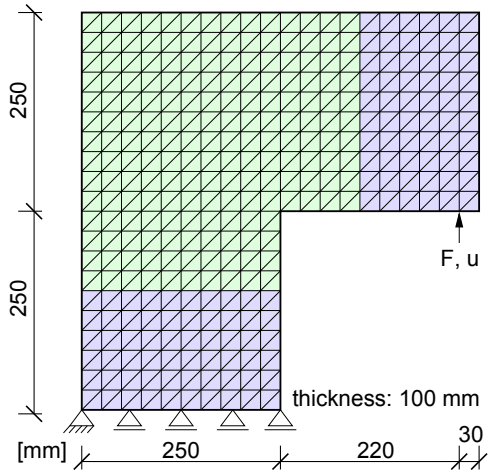

Figure 10: L-panel: system dimensions and finite element mesh (initial macroscale model).

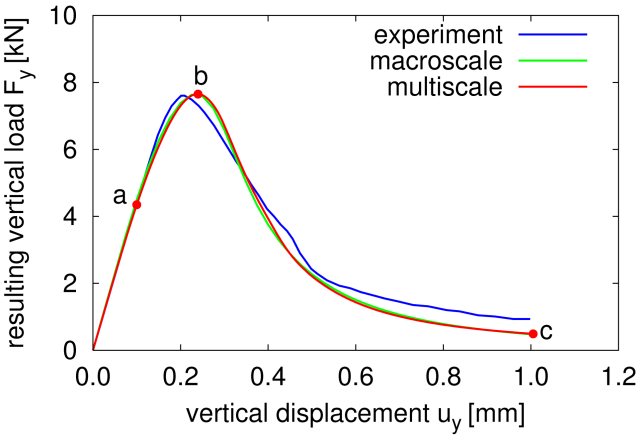

Figure 11: L-panel: global load displacement curve.

in the macroscale model and to the mortar matrix elements in the multiscale model. Furthermore rigid bond between aggregates and matrix and linear eleastic behavior of the aggregates is assumed. A fitting of the material parameters to the experimental results is performed for the macroscale model. Then the material parameters of the mesoscale model are derived from the macroscale model. The Reuss bound [17] is used for the calculation of the Young's modulus:

$$\frac{1}{E_c} = \frac{\varphi_a}{E_a} + \frac{\varphi_m}{E_m} \tag{23}$$

where E is the Young's modulus, φ is the area fraction and the subscripts stands for concrete (macroscale): c, aggregates: a and mortar matrix: m. In the presented simulations only aggregates of the mineral-size classes $2/4$ and $4/8$ with a volume fraction of $17\ \%$ are considered. This results in the two dimensional model in an area fraction of $15\,\%$. Furthermore it is assumed that the Young's modulus of the aggregates is twice the Young's modulus of the mortar matrix. The resulting material parameters are given in Table 2.

Table 2: L-panel: material parameters.

		Concrete	Mortar	Aggregates
E	$[N/mm^2]$	20,000	18,500	37,000
ν	$[-]$	0.18	0.18	0.18
f_t	$[N/mm^2]$	2.2	2.2	–
G_f	$[N/mm]$	0.155	0.155	–
R	$[mm]$	10	1	–

The pure macroscale model consists of 4188 triangular elements with quadratic interpolation functions and 8577 nodes. A mean element size of 5 mm is chosen within the damaged region. The whole analysis takes approximately 3 minutes on an Opteron workstation with 2.4 GHz.

Figure 10 illustrates the initial macroscale finite element discretization, 600 elements and 1281 nodes, for the multiscale analysis. A mean element size of 25 mm on the macroscale and 0.75 mm on the mesoscale is chosen. An adaptation of the macroscale model is only allowed in the green marked part of the model. After the first model adaptation the finite element mesh consists of 32,253 elements and 63,853 nodes. The evolution of the mesoscale substructure

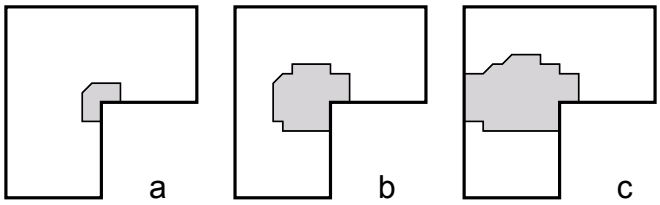

Figure 12: Model adaptation: initial state (a), at the maximum load level (b), final state (c).

with respect to the global load-displacement diagram (Figure 11) is shown in Figure 12. In the final state the model is represented using 173,278 elements and 352,101 nodes. The nonlinear analysis with the adaptive heterogeneous multiscale model takes approximately 12 hours on the Opteron workstation. Calculation of the element stiffness matrices and assembling of the global stiffness matrix is performed on 4 parallel processors.

The global load displacement curves are plotted in the diagram in Figure 11. Both models can reproduce the experimentally observed curve. Differences can be seen in the position of the peak point. In both simulations the displacement corresponding to the peak load is a little bit too large (about $\sim 5\,\%$). Nearly no difference can be seen in the load-displacement curves of the two simulations. This is a result of the size of the structure. The loss of stiffness due to the initiation and propagation of microcracks, which is covered by the multiscale model, cannot be recognized in the global load-displacement curve. Only the formation and propagation of a macroscopic crack results in a noticeable nonlinear behavior of the response curve.

Large differences between both models can be seen in the damage distribution shown in Figure 13. In the macroscale model the simulation results in a straight horizontal crack path. The width of the damage zone corresponds to the nonlocal interaction radius of the isotropic damage model. A more realistic crack path is observed using the multiscale model. On the mesoscale the initiation and propagation of microcracks and the formation of the macroscopic crack can be explicitly observed during the simulation. The macroscopic crack is bridging from aggregate to aggregate which results in a curved shape of the crack. In addition to the macroscopic dominating crack several smaller cracks are built. The width of the damage zone is highly influenced by the heterogeneous material structure on the mesoscale. It is significantly

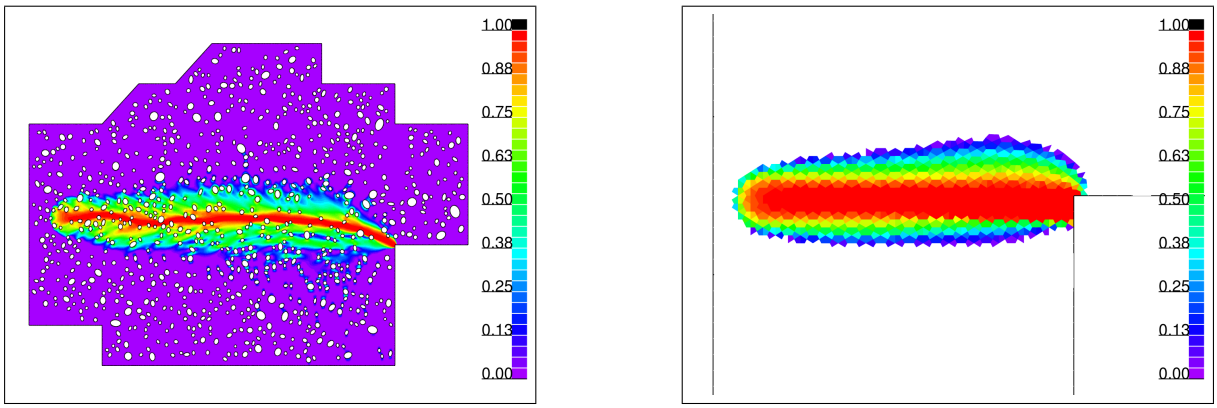

(a) multiscale model (detail mesoscale)

(b) macroscale model (detail damage zone)

Figure 13: L-panel: damage distribution, final state.

larger than the chosen nonlocal interaction radius and is comparable to the width observed in the macroscale model.

4 CONCLUSIONS

In the first part of the paper a mesoscale model of concrete, considering the nonlinear behavior of the mortar matrix and the ITZ has been introduced. This model has been applied to the nonlinear simulation of a uniaxial tension test of a concrete prism. The used nonlocal isotropic damage model can represent the initiation, propagation and coalescence of microcracks on the mesoscale and the resulting formation of a macroscopic crack. Considering the nonlinear behavior of the ITZ a better approximation of the experimentally observed pre-peak behavior of concrete is represented, compared to a simulation assuming rigid bond.

In the second part of the paper an adaptive heterogeneous multiscale approach for the simulation of damage in concrete structures has been introduced and successfully applied to the nonlinear analysis of a realistic structure. Modeling only the damaged regions of the structure on the mesoscale results in numerical models, that can be handled with today's computational power. The obtained numerical results show a good agreement with the experiment. Compared to a pure macroscale simulation of the specimen the analysis with the multiscale model results in a more realistic crack pattern.

In the future the stochastic character of the mesoscopic geometry as well as material parameters has to be taken into account. In the adaptive multiscale approach the coarsening of the model, that is the transfer from the meso- to the macroscale, has to be considered. Homogenization techniques, which calculate the average macroscopic material tensor from the mesoscopic damage distribution, are currently developed. For realistic simulations of concrete structures an extension to three-dimensional models is definitely necessary.

ACKNOWLEDGEMENT

This research has been supported by the German Research Foundation (DFG) through Collaborative Research Center 524, which is gratefully acknowledged by the authors.

REFERENCES

[1] M. Jirásek and Z.P. Bažant. *Inelastic Analysis of Structures*. Wiley, 2002.

[2] Z.P. Bažant and J. Planas. *Fracture and size effect in concrete and other quasibrittle materials*. CRC Press, 1997.

[3] G. Hofstetter and H.A. Mang. *Computational Mechanics of Reinforced Concrete Structures*. Vieweg, 1995.

[4] E. Schlangen and J.G.M. van Mier. Experimental and numerical analysis of micromechanisms of fracture of cement-based composites. *Cement and Concrete Composites*, 14(2):105–118, 1992.

[5] V. Slowik and J.P. de Barros Leite. Meso-level modelling of concrete fracture. In *Leipzig Annual Civil Enegineering Report, LACER No. 5*. University of Leipzig, 2000.

[6] S. Eckardt, S. Häfner, and C. Könke. Simulation of the fracture behaviour of concrete using continuum damage models at the mesoscale. In *Proc. of the 4th ECCOMAS*, 2004.

[7] S. Häfner, S. Eckardt, T. Luther, and C. Könke. Mesoscale modeling of concrete: geometry and numerics. *Computer & Structures*, 84(7):450–461, 2006.

[8] W. Wang, W. Jiaye, and K. Myung-Soo. An algebraic condition for the separation of two ellipsoids. *Computer aided geometric design*, 18(6):531–539, 2001.

[9] B. Patzák and M. Jirásek. Adaptive resolution of localized damage in quasibrittle materials. *Journal of Engineering Mechanics ASCE*, 130:720–732, 2004.

[10] M. Jirásek and B. Patzák. Consistent tangent stiffness for nonlocal damage models. *Computers & Structures*, 80:1279–1293, 2002.

[11] P.R. Amestoy, I.S. Duff, and J.-Y. L'Excellent. Multifrontal parallel distributed symmetric and unsymmetric solvers. *Computer Methods in Applied Mechanics and Engineering*, 184(2-4):501–520, 2000.

[12] V. Tvergaard. Cohesive zone representations of failure between elastic or rigid solids and ductile solids. *Engineering Fracture Mechanics*, 70:1859–1868, 2003.

[13] J.F. Unger and C. Könke. Simulation of concrete using the extended finite element method. In G. Meschke, R. de Borst, H. Mang, and N. Bićanić, editors, *Computational Modelling of Concrete Structures, EURO-C*, 2006.

[14] C. Kessler-Kramer. *Zugtragverhalten von Beton unter Ermdungsbeanspruchung*. PhD thesis, Universitt Karlsruhe (TH), 2002.

[15] C. Geuzaine and J.-F. Remacle. *Gmsh Reference Manual*. 2005.

[16] B. Winkler. *Traglastuntersuchungen von unbewehrten und bewehrten Betonstrukturen auf der Grundlage eines objektiven Werkstoffgesetzes für Beton*. PhD thesis, University of Innsbruck, Austria, 2001.

[17] A. Reuss. Berechnung der Fliessgrenze von Mischkristallen auf Grund der Plastizitätsbedingung für Einkristalle. *Z. Angew. Math. Mech.*, 9:49–58, 1929.